

# Multi-Scale Cell Decomposition for Path Planning using Restrictive Routing Potential Fields

Josue N. Rivera, Dengfeng Sun  
School of Aeronautics and Astronautics  
Purdue University  
West Lafayette, IN, USA  
{river264, dsun}@purdue.edu

**Abstract**—In burgeoning domains such as urban goods distribution, the advent of aerial transportation necessitates the development of routing solutions that prioritize safe navigation. This paper introduces Larp, a novel path planning and navigation framework that leverages the concept of repulsive potential fields as continuous cost maps to forge safe routes. The algorithm achieves it by segmenting the potential field into a hierarchy of cells, each with a designated risk zone determined by the proximity of obstacles. The meshing allows the airspace to be partitioned based on an area's potential for restriction violations, enabling navigation that is aware of these risks. While the primary impetus behind Larp is to enhance the safety of aerial pathways for Unmanned Aerial Vehicles (UAVs) in urban air mobility, its utility extends to a wide array of routing scenarios. Comparative analyses with both established and contemporary potential field-based methods reveal Larp's proficiency in maintaining a safe distance from restrictions and its adeptness in circumventing local minima. Additionally, large-scale aerial path planning of Austin, TX demonstrates Larp's capability to be implemented at a large scale.

**Keywords**—potential field; cost maps; air traffic management; path planning; unmanned aerial vehicle; urban air mobility

## I. INTRODUCTION

As we look to the future, the role of aerial cargo delivery is expected to become central in the domain of urban goods transportation. Given its growing importance, the development of solutions that are both scalable and verifiably safe is crucial [1]–[4]. Routing solutions are integral to this aspect. The flight paths chosen for unmanned aerial vehicles (UAVs) significantly influence the potential for aerial incidents. Consequently, a route's function now extends beyond mere connectivity from origin to destination; it must also encompass considerations for safety.

This paper introduces Larp, a path planning and navigation framework tailored for restrictive routing within potential fields as cost maps. The framework decomposes a potential field into multi-scale cells, each with an estimated maximum potential for its region, and utilizes graph path planning algorithms to generate routes that overcome several issues associated with traditional artificial potential field methods. Although primarily conceived to bolster the safety and scalability of UAV-operated aerial cargo transport within urban air mobility (UAM), the algorithm's utility extends beyond this scope. It is versatile enough to be implemented in any setting that aligns with the potential field standard to be discussed [5].

## A. Background

Cost maps in path planning describe a routing scheme in which sectors of a map are assigned a cost or penalty for being in a particular region, and routes are formulated to minimize the accumulated cost of navigation [6], [7]. These maps are utilized in mobile robotics for path planning with risk assessment to effectively navigate obstacles [7], [8]. Urban air mobility, a multifaceted endeavor, necessitates the consideration of various factors, including obstacle clearance, noise pollution, privacy concerns, and ground risks [4], [9]. Cost maps serve as a powerful tool to represent general restriction violations by abstracting the complexity of risk assessment into a spatial cost metric. They have shown significant promise for UAV path planning based on risk assessment [6], [10]–[12]. Demonstrated benefits include reducing risks in metropolitan areas, integrating multiple risk factors into a single cost map, and aiding in prioritizing search areas during search-and-rescue missions. Another critical avenue explored is the inclusion of airspace occupancy in cost maps, facilitating routing that minimizes conflicts with other aerial vehicles operating in the same airspace [13], [14].

Artificial potential fields define a continuous mathematical system with attractive and repulsive forces that move particles towards a goal. Areas to avoid are classified as having high repulsive potential that decays with distance from the particle. Traditionally, path planning with potential fields involves simulating particles influenced by the repulsive field while being attracted towards the goal via an attractive force [15]–[23]. These fields are utilized for a variety of autonomous vehicles. In dynamic environments, potential fields have been used to guide the navigation of autonomous underwater vehicles (AUVs) with moving obstacles [24]. Potential fields have also shown promise for UAV path planning in both simulation and real-world environments [15], [16], [25], [26]. Their use has led to increased safety by ensuring a maintained distance from obstacles and, at times, faster path searches due to the system's simplicity and its heuristic nature. However, research on artificial potential fields for UAVs is limited [27]. The main drawback of potential field methods is that they may form local minima that impede agents from reaching their destination. From one perspective, the repulsive component of a potential field can be classified as a class of continuous cost maps, defined in a space where any point in the field has

a potential that must be minimized. We seek to combine this concept with variable resolution cost maps to generate safer routes in complex continuous spaces.

Similar to our work, [15], [16] investigate the application of potential fields for path planning, with [15] specifically utilizing them to quantify safety. These studies also employ graph-based algorithms such as A\* to navigate around local minima, a well-known issue associated with artificial potential field (APF) methods. However, the methodology of [15] is confined to fixed grid-based environments, and [16] primarily applies A\* within a grid context to overcome local minima, which may lead to routes that are not optimized for distance. While cell decomposition has widespread use for environment representation in UAV operations, few studies consider artificial potential fields [27]. We propose a framework for cell decomposition that relies on artificial potential fields as cost maps. This approach allows for the examination of variable proximity to obstacles using an analytical method for multi-resolution cell decomposition and the assignment of safety guidelines to routes based on the expected accumulated potential. Moreover, a significant portion of the reviewed works focus on grid-based environments, which may not accurately reflect real-world situations. Our work operates in both continuous and complex spaces through a standardized format.

## II. PRELIMINARIES

### A. Restrictive Routing Potential Fields

In [5], we explore the problem of last-mile UAVs air traffic management and aerial cargo delivery in urban environments, and introduce a standard for restrictive routing using cost map based on repulsive artificial potential fields. Assuming a constant operating altitude, physical and virtual restrictions are designated as areas of high potential that diminishes the further an UAV (or agent) is from an obstacle; a behavior dictated by their repulsion matrix.

The standardization facilitates an uniform approach to cost map construction, enabling consistent replication and analysis across different routing algorithms. By leveraging the structured nature of the potential field, such algorithms can efficiently navigate through complex environments utilizing a common standard, avoiding obstacles, and minimizing the risk of restriction violations. Additionally, it serves as a foundation for urban air traffic management and to analyze and study bottlenecks in the feasible airspace. The potential field delineated herein is henceforth denoted as a ‘restrictive routing potential field’.

### B. Standardized Potential Field Units

Under the proposed standard, a restrictive routing potential field is comprised of multiple building block units, each corresponding to a distinct type of restriction. Upon examining their definitions, a set of intrinsic properties emerges: a repulsion vector  $\bar{x}$ , a scaled squared distance  $\tilde{d}^2(x)$ , and a potential evaluation  $\sigma(x)$ . The repulsion vector  $\bar{x}$  encodes the direction from and proximity to the restricted areas. The scaled squared distance  $\tilde{d}^2(x)$  reflects the weighted proximity to a point  $x$ , modulated by the unit’s repulsion matrix  $A$ .

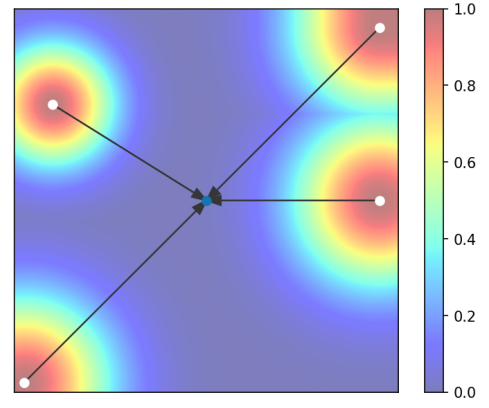


Figure 1: Illustration of the repulsion vectors with respect to a location.

Finally, the potential  $\sigma(x)$  denotes the field’s influence at point  $x$ , effectively reflecting the potential for restriction violation.

The repulsion vectors for the fundamental units and collection of them are detailed in Table I. Fig. 1 illustrate the repulsion vectors for an arbitrary set of obstacles with respect to an arbitrary point. The magnitude of each vector indicates proximity to the obstacle and the direction provides a guide towards moving away from it.

**Definition 1** (Squared Distance to a Potential Field Unit). A proxy to the squared distance to a potential field unit  $d^2(x)$  is defined as:

$$d^2(x) = \bar{x}(x)^T \bar{x}(x),$$

where  $\bar{x}(x)$  is the repulsion vector detailed in Table I and  $x$  is an evaluated point. For a collective of units,  $d^2(x)$  is the smallest squared distance among all sub-units.

**Definition 2** (Scaled Squared Distance to a Potential Field Unit). The scaled squared distance to a potential field unit  $\tilde{d}^2(x)$  is defined as:

$$\tilde{d}^2(x) = \bar{x}(x)^T A^{-1} \bar{x}(x),$$

where  $\bar{x}(x)$  is again the repulsion vector from Table I,  $A$  is the positive definite repulsion matrix of the unit, and  $x$  is an evaluated point. In the case of a collection of units,  $\tilde{d}^2(x)$  is the minimum of the scaled squared distances with respect to its sub-units.

**Definition 3** (Potential of an Unit). The potential of a unit  $\sigma(x)$  is defined as the exponential of the scaled squared distance to the unit:

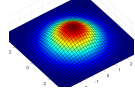
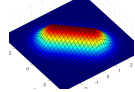
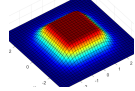
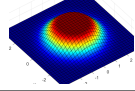
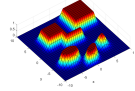
$$\sigma(x) = \exp(\tilde{d}^2(x)),$$

where  $\tilde{d}^2(x)$  is the scaled squared distance, and  $x$  is an evaluated point.

## III. METHODOLOGY

Given the properties of the standardized potential field, we introduce Larp (Last-mile restrictive path planning) as a routing framework for safe path planning and navigation.

TABLE I. Restrictive Routing Potential Field Units

Unit	Parameters	Repulsion vector $\bar{x}(x)$	Field
Point	Location $\hat{x}$ Repulsion matrix A	$\bar{x}_p(x) = x - \hat{x}$	
Line	Line start $\hat{x}_1$ Line end $\hat{x}_2$ Repulsion matrix A	$\rho(x) = \frac{(\hat{x}_2 - \hat{x}_1) \cdot (x - \hat{x}_1)}{\ \hat{x}_2 - \hat{x}_1\ ^2}$ $\bar{x}_l(x) = x - \hat{x}_1 + \text{clamp}(\rho(x), 0, 1)(\hat{x}_2 - \hat{x}_1)$	
Rectangle	Corner $\hat{x}_1$ Opposite corner $\hat{x}_2$ Repulsion matrix A	$g(x) = \frac{1}{2}( x - \hat{x}_1  +  x - \hat{x}_2  -  \hat{x}_1 - \hat{x}_2 )$ $\bar{x}_r(x) = \text{sign}(x - \hat{x}_1) \odot g(x)$	
Ellipse	Location $\hat{x}$ Repulsion matrix A Ellipse shape matrix B	$\bar{x}_e(x) = \max\left(1 - \frac{1}{\ B^{-1}(x - \hat{x})\ }, 0\right)(x - \hat{x})$	
Collection	Parameters of the sub units	Repulsion vector $\bar{x}(x)$ of sub unit with smallest scaled squared distance $\bar{d}^2(x)$	

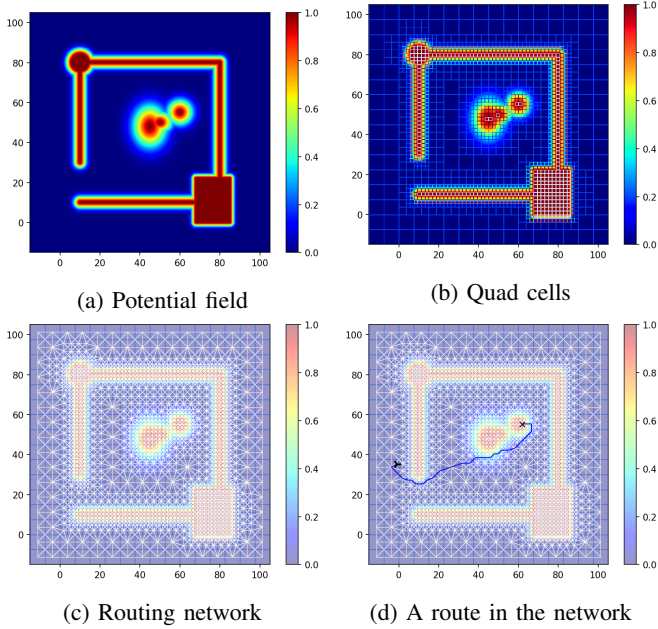


Figure 2: Stages of Larp for a walled room scene

It consists of three main stages: first, a core algorithm that decomposes a field into distinct multi-scale cells; secondly, the formation of a routing network using the cells and their adjacency; lastly, the search for a feasible, suitable, and safe route. The stages can be observed in Fig. 2.

Note that an official implementation of Larp can also be found on our Github repository at <https://github.com/wzjoriv/Larp>.

#### A. Multi-Scale Cell Decomposition

Drawing inspiration from adaptive quad tree cell decomposition, the first and main phase consists of partitioning a potential field into a multitude of cells, each varying in

size. These cells are then correlated with their respective potential for infringing nearby restrictions. The stratagem for cell subdivision is calibrated, ensuring that cells proximal to obstacles are proportionately smaller, thereby augmenting routing precision and safety. Fig. 2b illustrates this decomposition for a walled room scene. The methodology behind cell decomposition is expounded in Algorithms 1 and 2.

1) *Cells Quad Tree Structure*: Algorithm 1 consists of a recursively subdividing a field into quadrants (i.e., quad or cell) and assigning a restriction zone based on the area potential for violating a restriction. This forms a tree structure with quad cells as node. The tree allows for quick search of any area and the restrictions in it. An example of the quad tree structure is presented in Fig. 3 for a simple field. Initially, at the start of the algorithm, an empty node is initialize for the current observed quadrant. Then, via Algorithm 2, and the highest (i.e., closest) risk zone is assigned from a list of maximum potential limits. Once a zone has been assigned, it is determined whether the subdivision should stop or continues. It stops if we have assigned the further zone allowed or the minimum desired cell size has been reached. After that, we remove any obstacle from consideration that is too far from the quadrant and subdivide again for each quadrant inside the current sector. The leaves of the generated tree present the multi-scale cell decomposition of the potential field and the individual restriction zone.

2) *Repulsion Vectors and Potential of an Area*: The heart of the cell decomposition is estimating the maximum potential of any cell in the potential field and assigning a restriction zone. This is done by Algorithm 2. By relying on the intrinsic properties of the standardized potential field, an maximum potential to violate restrictions can analytically be determined. Initially, we calculate a proxy of the square distance of each obstacle unit with respect to the center of a quad. If the distance is less than the radius of the circumscribed circle of the quad, then the obstacle is assigned zone 0 (i.e., an

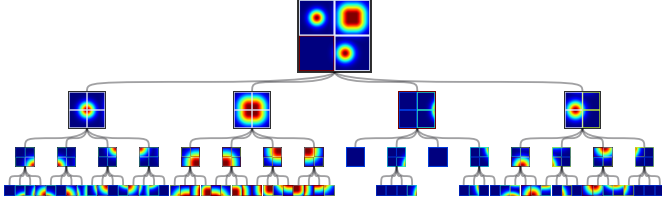


Figure 3: Quad tree for a simple potential field.

---

**Algorithm 1** Larp – Quad Tree Cell Decomposition

---

```

1: function BUILD( $x, n, U$ )
2:    $quad \leftarrow QuadNode(x, n)$ 
3:    $zones \leftarrow$  map with default farthest zone
4:   if  $|U| > 0$  then
5:      $zones \leftarrow APPROXOBSTACLESZONES(x, n, U)$ 
6:   end if
7:    $quad.zone \leftarrow \min(zones) \triangleright$  Farthest zone if empty
8:   if  $n \leq n_{max}$  then
9:     if  $n \leq n_{min}$  or  $quad.zone$  is farthest zone then
10:      Mark  $quad$  as leaf
11:      return  $quad$ 
12:     end if
13:   end if
14:    $U \leftarrow \{u \in U \mid zones[u] < \text{farthest zone}\}$ 
15:   for each quad  $q$  of a cell do
16:      $quad.child[q] \leftarrow BUILD(q.center, n/2, U)$ 
17:   end for
18:   return  $quad$ 
19: end function
20:  $root \leftarrow BUILD(\text{field.center}, \text{field.size}, \text{all units in field})$ 

```

---

obstacle exist in the area). Trivially, this ensures that if an obstacle is in the area, it is classified as being in zone 0. For the other zones, we must rely on the scaled distance to the obstacles. First, we use the repulsion vector of each obstacle to estimate a location  $c$  of where the obstacle is closest to the area. Then, we sample the potential at this location for each obstacle individually and assign it to a zone based on how close they are to the value 1.0. Each zone assignment is based the potential of any obstacle to be violated by an agent in the area (or indirectly their weighted proximity of the sector to the restriction).

Fig. 4 illustrates how an area maximum potential (or risk) zone can be approximated. First, the repulsion vector of each obstacle is flipped and clamped to the magnitude of the diagonal distance from the quad’s center to to its edge. In the figure, they are drawn from the center of the area and colored based on the maximum potential assigned. The maximum potential ranges for this example are ticked in the color bar. As the potential for the obstacle to the right of the center is the closest to 1.0, the entire circular area is estimated to have an maximum potential of 0.8. As a subset of the circular area, the quad is also estimated to have an maximum potential upper limit of 0.8.

---

**Algorithm 2** Larp – Estimate Maximum Potential Zone of a Quad

---

**Require:** Sorted list of boundaries  $bds$  in descending order

```

1: function APPROXOBSTACLESZONES( $x, n, U$ )
2:    $zones \leftarrow$  map with default farthest zone
3:   for each unit  $u$  in  $U$  do
4:     if  $d_u^2(x) \leq \frac{n^2}{2}$  then
5:        $zones[u] \leftarrow 0$ 
6:     end if
7:   end for
8:   for each unit  $u$  in  $U$  but not already in  $zones$  do
9:      $c = x - \frac{n}{\sqrt{2} \|\bar{x}_u(x)\|} \bar{x}_u(x)$ 
10:     $p = \exp\left(\frac{n^2}{2} d_u^2(c)\right)$ 
11:    Assign  $zones[u]$  into bin given  $bds$  and  $p$ 
12:   end for
13:   return  $zones$ 
14: end function

```

---

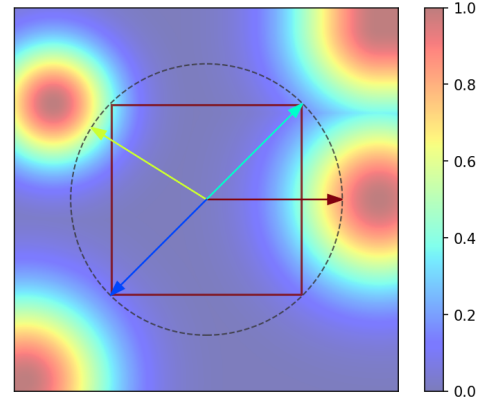


Figure 4: Estimating the maximum potential of an given area in the potential field.

### B. Routing Network

To streamline path planning within the designated space, a network graph is constructed subsequent to the potential field’s decomposition. The process employs a divide-and-conquer approach to traverse the quad tree, facilitating the identification of neighboring nodes for any given leaf quad node. The intricacies of the field are distilled into a simplified network, where each graph node correlate with a leaf cell and its maximum potential for the vicinity. Fig. 2c provides a visual representation of this network graph.

In the interest of brevity, we have omitted the detailed adjacency algorithm used to construct the routing network; however, it is available for review in our public repository.

### C. Path Planning

Upon the establishment of the network, the implementation of any graph routing algorithm that simultaneously minimizes route distance and accumulated potential is applicable. For this study, we employ a modified variant of the renowned A\* algorithm, wherein the distance function is redefined as:

$$d(q_a, q_b) = s(q_b) \cdot \|q_a.\text{center} - q_b.\text{center}\| \quad (1)$$

where  $q_a$  and  $q_b$  denote the quadrant being traversed from and to, respectively;  $s(q)$  represents scale transformation function that modulates the penalty of going to a new sector given its maximum potential; and  $q_a.\text{center}$  signifies the centroid of a cell  $q_a$ . A route generated for the walled room scene is depicted in Fig. 2d. Subsequent to determining a routing solution, line segments are integrated to connect the initial location and the destination with the discovered route within the network.

#### D. Safety Validation

It is imperative to establish a commonality for defining what constitutes a route within a potential field to assess effectiveness of the routing solutions.

**Definition 4** (Route in a Potential Field). *A route  $R$  within a restrictive routing potential field is delineated as a trajectory comprising a line string that interconnects a sequence of points, expressed as:*

$$R_p = \{x_1, x_2, \dots, x_N\}$$

where  $x_i$  signifies a 2D coordinate in a plane, and  $N - 1$  represents the count of consecutive line segments that constitute the line string.

With Definition 4 established, several metrics to evaluate the safety of a route can be examined. The primary metric is the cumulative potential under a route's trajectory, calculated as:

$$R_A = \int_R \sigma(x_t) dx_t = \sum_{i=0}^{N-1} \int_{x_i}^{x_{i+1}} \sigma(x_t) dx_t \quad (2)$$

where  $\sigma(\cdot)$  denotes the potential field assessment, and  $\int_{x_i}^{x_{i+1}} \sigma(x_t) dx_t$  encapsulates the line integral from point  $x_i$  to point  $x_{i+1}$ . This metric gauges the aggregate potential for committing a restriction violation by an agent traversing the route, with higher values indicating increased interaction with restricted regions.

Conversely, a route's length as a measure of safety is considered:

$$R_d = \int_R 1 dx_t = \sum_{i=0}^{N-1} \int_{x_i}^{x_{i+1}} 1 dx_t \quad (3)$$

The extended duration of a route implies a prolonged presence within the field, elevating the risk of violation occurrences.

Ultimately, combining these two metrics yields a composite measure that reflects the average engagement with restrictions along a route

$$R_{avg} = \frac{R_A}{R_d} \quad (4)$$

A heightened  $R_{avg}$  value suggests a route's active proximity to restricted areas. Empirical observations indicate that a threshold of 0.35 or below is typically indicative of minimal engagement with restrictions.

## IV. EXPERIMENTS AND RESULTS

### A. Potential field-based path planning algorithms

To assess the efficacy of our algorithm, we have compiled a suite of path planning strategies that leverage potential fields to evaluate proximity to obstacles and violating routing restrictions. Detailed implementations and comparisons of these methods are available in our Github repository at <https://github.com/wzjoriv/path-planning-pf>.

1) *Penalty Method with Gradient Descent (PM)*: The penalty method with gradient descent introduces an attractive force that propels an agent towards a goal, defined as:

$$F_A(x) = \zeta(x_g - x) \quad (5)$$

where  $\zeta$  is a scalar hyper-parameter dictating the strength of the attraction, and  $x_g$  denotes the goal's location. Additionally, a repulsive force emerges from a penalty on the potential field value,

$$F_R(x) = -\eta p'(\sigma(x)) \nabla \sigma(x) \quad (6)$$

where  $\eta$  is a scalar hyper-parameter governing the repulsion,  $p'(\cdot)$  is the derivative of the penalty function, and  $\nabla \sigma(x)$  represents the gradient of the potential field under discussion.

Combining these two forces forms a traversal strategy that steers the agent towards the goal, articulated as:

$$x_{i+1} = x_i + \gamma \frac{F_A(x_i) + F_R(x_i)}{\|F_A(x_i) + F_R(x_i)\|} \quad (7)$$

where  $\gamma$  signifies the step size, and  $x_0$  is the agent's initial location. To circumvent local minima near the goal, our experiments introduce a heuristic: if  $\|x_N - x_g\| \leq 2.5$ , a direct line segment to the goal  $x_g$  is appended to the route's  $R_p$ .

2) *Artificial Potential Field (APF, APF(\*))*: The classical APF method supplants the gradient-based approach with a traditional repulsive force as delineated in [22], [23]. Within the scope of the problems addressed, this repulsive force is articulated by:

$$F_R(x) = \begin{cases} \eta \left( \frac{1}{d(x)} - \frac{1}{d_o} \right) \frac{1}{d^2(x)} \bar{x}(x), & \text{if } d(x) \leq d_o \\ 0, & \text{otherwise} \end{cases} \quad (8)$$

where  $d(x) = \sqrt{d^2(x)}$ ,  $d_o$  is the threshold distance at which the repulsive force becomes active, and  $\bar{x}(x)$  is the repulsion vector from the nearest obstacle.

Subsequent enhancements to the APF methodology, not originally included but recommended for improved efficacy, propose an alternative attraction force [22]:

$$F_A(x) = \begin{cases} \zeta(x_g - x), & \text{if } \|x - x_g\| \leq d_g \\ \zeta d_g \frac{x_g - x}{\|x - x_g\|}, & \text{otherwise} \end{cases} \quad (9)$$

where  $d_g$  is the critical distance beyond which the attraction force adopts a quadratic profile to ensure a smooth convergence to the target.

For the APF method, a variant denoted as APF (\*) is also implemented for which square distance function  $d^2(x)$  is substituted with its scaled counterpart  $\tilde{d}^2(x)$ .



TABLE II. Performance metrics for Scenario 1. All algorithms successfully reach the goal. Larp generates a slightly longer path due to its conservative movements and emphasis on safety. A  $\checkmark$  under 'Goal Found' indicates  $\|x_N - x_g\|^2 \leq 2.5$  where  $x_N$  is the final position of a route.

Algorithm	Goal Found	Distance ( $R_d$ )	Potential ( $R_A$ )	$R_{avg}$	Highest Potential
PM	$\checkmark$	62.04	0.4006	0.0065	0.0619
APF	$\checkmark$	62.06	0.3863	0.0062	0.0594
APF (*)	$\checkmark$	<b>62.02</b>	0.4020	0.0065	0.0622
M-APF	$\checkmark$	<b>62.02</b>	0.4020	0.0065	0.0622
Larp (Our)	$\checkmark$	62.9181	<b>0.1082</b>	<b>0.0017</b>	<b>0.0084</b>

3) *Modified Artificial Potential Field (M-APF)*: M-APF, an advanced iteration of APF introduced by [20], [21], innovates upon the conventional repulsion force to mitigate the issue of local minima. The reformulated force is expressed by:

$$F_{R1}(x) = \eta \left( \frac{1}{d(x)} - \frac{1}{d_o} \right) \|x - x_g\|^{m-3}$$

$$F_{R2}(x) = \eta m \left( \frac{1}{d(x)} - \frac{1}{d_o} \right)^2 \|x - x_g\|^m \quad (10)$$

$$F_R(x) = \begin{cases} F_{R1}(x) + F_{R2}(x) \frac{\bar{x}(x)}{\|\bar{x}(x)\|}, & \text{if } d(x) \leq d_o \\ 0, & \text{otherwise} \end{cases}$$

where  $m$  is a positive scalar hyper-parameter that modulates the repulsion force's sensitivity to the agent's proximity to the goal.

### B. Results: Routes in a small room

In evaluating these algorithms, we explored three distinct scenarios of path planning in a small room.

1) *Scenario 1 (Unobstructed Path)*: The first scenario considers a straightforward path planning task where the objective is to travel towards an unobstructed target. Although there are no significant obstacles present, this scenario serves to accentuate the subtle differences between the algorithms. As shown in Table II and Fig. 5, even in an ideal situation where no obstacles impede the path, Larp—placing a premium on safety—may yield routes that are marginally longer if it results in a lower overall potential energy.

2) *Scenario 2 (Obstructed Path and Near-Obstacle Goal)*: This scenario examines the algorithms' performance when an agent must navigate around an obstacle and when the target is in close proximity to one. The results are presented in Table III and Fig. 6. When obstacles are introduced along the route, both PM and APF struggle to maintain a safe distance from the constraints, resulting in higher peak potential values. PM's dependence on gradients and penalties hinders its ability to significantly deviate from the obstacle's path. APF's higher potential can be attributed to its focus on immediate obstacle proximity rather than the overall potential for obstacle avoidance; however, it also contributes to its shorter route distance. Among all the methods evaluated, Larp consistently produced safer routes, albeit at the expense of increased distance. Nevertheless, Larp's route lengths remain competitive, particularly when compared to methods such as APF (\*) and M-APF.

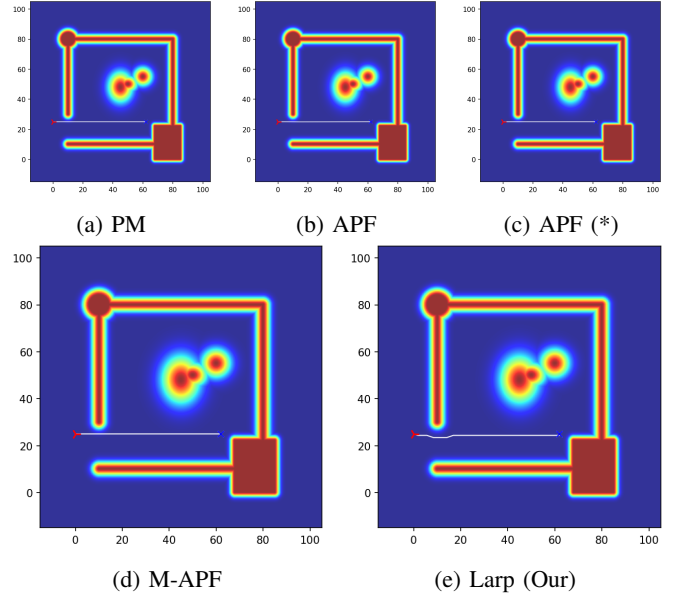


Figure 5: Comparison of routes in Scenario 1, featuring an unobstructed path. The red marker indicates the initial location of the agent.

TABLE III. Performance metrics for Scenario 2. The highest potential energy values for APF (\*), M-APF, and Larp reflect the goal's proximity to obstacles.

Algorithm	Goal Found	Distance ( $R_d$ )	Potential ( $R_A$ )	$R_{avg}$	Highest Potential
PM	$\checkmark$	79.188	23.1432	0.2923	0.9011
APF	$\checkmark$	<b>77.2863</b>	23.011	0.2977	0.9220
APF (*)	$\checkmark$	87.8328	29.3081	0.3337	<b>0.8948</b>
M-APF	$\checkmark$	80.8579	21.0194	0.26	<b>0.8948</b>
Larp (Our)	$\checkmark$	83.8675	<b>15.8687</b>	<b>0.1892</b>	<b>0.8948</b>

3) *Scenario 3 (Walled-Off Path)*: The final scenario investigates the behavior of the methods when the direct route to a target is obstructed by a wall. As depicted in Table IV and Fig. 7, all methods, except for Larp, fail to reach the destination. When confronted with non-circular restrictions, both penalty-based and force-based methods may struggle to overcome the local minima created by the opposing forces of attraction and repulsion from the obstacles.

TABLE IV. Performance metrics for Scenario 3. Except for Larp, all other methods are unable to reach the target; therefore, their performance measurements are not valid for comparison but provide insight into their behavior. In this table, an  $\times$  under 'Goal Found' indicates  $\|x_N - x_g\|^2 > 2.5$

Algorithm	Goal Found	Distance ( $R_d$ )	Potential ( $R_A$ )	$R_{avg}$	Highest Potential
PM	$\times$	33.32	18.6015	0.5583	0.9529
APF	$\times$	42.83	26.3972	0.6163	0.9075
APF (*)	$\times$	80.37	53.9457	0.6712	0.8075
M-APF	$\times$	38.57	1.8687	0.0485	0.0674
Larp (Our)	$\checkmark$	<b>163.8382</b>	<b>14.8769</b>	<b>0.0908</b>	<b>0.3453</b>

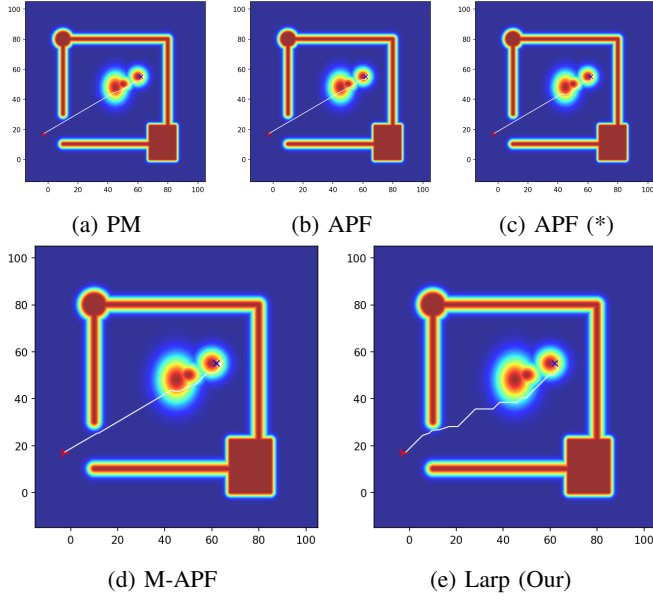


Figure 6: Scenario 2 of an obstructed path and near-obstacle goal (routes comparison)

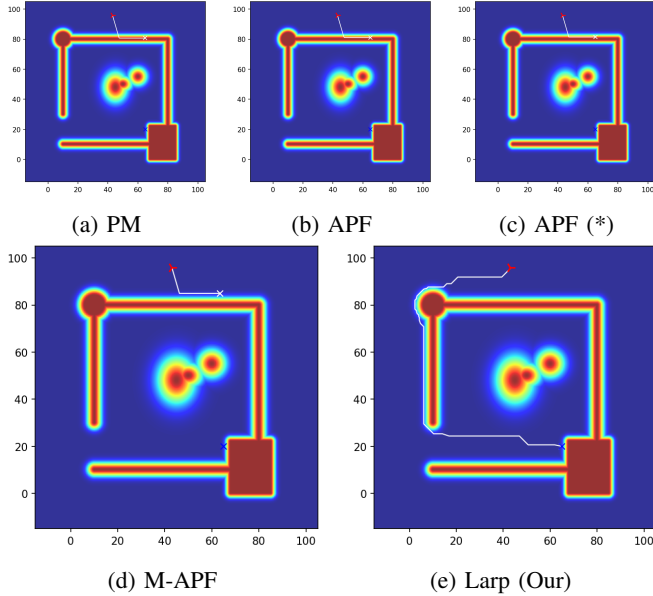
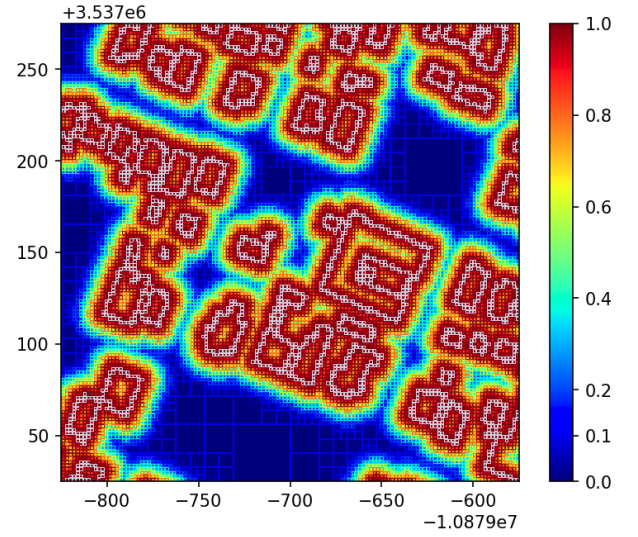


Figure 7: Routes comparison for Scenario 3, featuring a walled-off path.

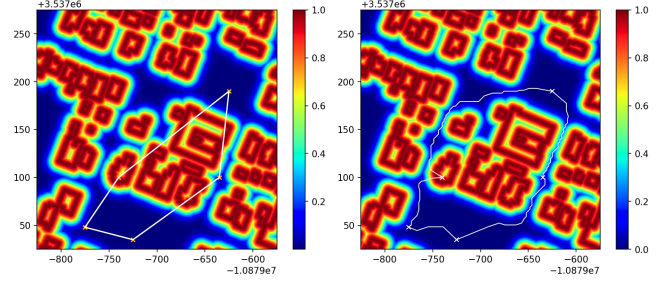
### C. Results: UAV routes in Austin, TX

Larp is capable of generating safe city-level routes. To test its capability, UAV routes for Austin, TX were generated using OpenStreetMap buildings data. It is assumed that all buildings are tall enough to interfere with UAVs travel, while anything outside of the area does not. Fig. 8 and 9 explore two similar but distinct scenarios involving urban air mobility.

In Fig. 8, travel within an urban environment is explored, specifically focusing on safe route generation inside a dense neighborhood with high buildings. As shown, Larp has the ability to generate routes that maintain a safe distance from building boundaries (colored deep red with a potential of



(a) Cell decomposition of dense neighborhood.



(b) Initial delivery points. (c) Routes generated by Larp.

Figure 8: Routes among high buildings in downtown Austin, TX.

one) wherever possible. It only enters a building's airspace when required to perform the delivery. Additionally, routes can adapt to crevices created by a number of buildings. Note that the scale of the axes is in meters, and the policy for proximity to buildings can be adjusted during path planning by the penalty function. For this demo, we have chosen to set an upper potential for restriction violation at 0.2, only getting closer when necessary without violating boundary restrictions.

Fig. 9 presents the results when the algorithm is expanded to a larger scale, including rural or unobstructed areas. In this scenario, the surrounding areas of Austin transition from a high dense urban sector to an unobstructed space. As observed, Larp generates coarse paths when away from buildings and granular paths when near them. The coarse paths allow for easier straight flights, which are convenient for long-distance travel without drastic maneuvering. When near a building, the granular, smoother, and more precise routes allow for safer navigation around the buildings. For the demonstration, and as illustrated, the routes for UAVs avoid buildings wherever possible. However, to ensure deliveries to buildings, we have opted to allow entrance into a building's airspace if necessary for delivery, as also seen in the previous

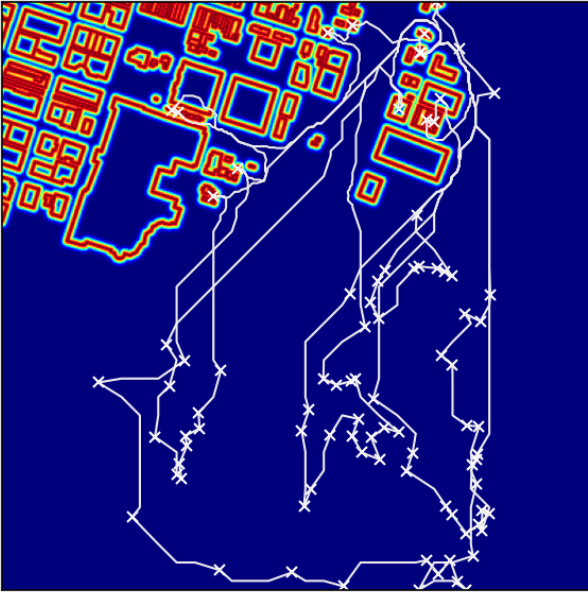


Figure 9: Routes surrounding downtown Austin, TX.

scenario.

The source code to generate the routes near Austin, TX or any city can be found on our Github repository at <https://github.com/wzjoriv/Larp>. A GeoJSON file of the city's buildings is needed to run it. It can be obtained via OpenStreetMap or similar map providers.

## V. CONCLUSION

This study introduces Larp, a novel path planning framework specifically designed for restrictive routing within potential fields. Larp has demonstrated superior performance compared to both traditional and contemporary potential field-based methodologies by consistently devising safer routes that mitigate the risk of restriction violations while maintaining competitive efficiency in terms of travel distance. Additionally, Larp has proven capable of assigning sector-specific risks and generating safety-aware routes at a city-wide scale. The routing solution dynamically adapts maneuverability based on the density of any given region. This success is achieved through the initial decomposition of a potential field into multi-scale cells, with each cell's restriction zone determined by its proximity to nearby obstacles. To promote transparency and support further research, the source code for an official implementation of Larp has been made publicly accessible at <https://github.com/wzjoriv/Larp>.

While Larp marks an advancement in UAV route safety, opportunities for improvement remain. The framework's quad cell decomposition approach and zone classification system are poised for further optimization. The influence of a cell's dimensions and positioning on the placement of subsequent cells is a critical factor in the pursuit of optimally short and safe routes. Moreover, the current method of zone classification, which relies on a proxy scaled distance to a cell's periphery to gauge the highest potential across the region, may estimate a significantly higher potential for a region

than what it actually is. Future endeavors will concentrate on refining these elements and developing a dynamic and scalable system capable of storing and updating cells in real time to adapt to evolving restrictions for unmanned aircraft system traffic management (UTM).

## REFERENCES

- [1] Rakesh Shrestha, Inseon Oh, and Shiho Kim. A survey on operation concept, advancements, and challenging issues of urban air traffic management. *Frontiers in Future Transportation*, 2:1, 2021.
- [2] Khaled Telli, Okba Kraa, Yassine Himeur, Abdelmalik Ouamane, Mohamed Boumechraz, Shadi Atalla, and Wathiq Mansoor. A comprehensive review of recent research trends on unmanned aerial vehicles (uavs). *Systems*, 11(8):400, 2023.
- [3] Bhawesh Sah, Rohit Gupta, and Dana Bani-Hani. Analysis of barriers to implement drone logistics. *International Journal of Logistics Research and Applications*, 24(6):531–550, 2021.
- [4] Aleksandar Bauranov and Jasenka Rakas. Designing airspace for urban air mobility: A review of concepts and approaches. *Progress in Aerospace Sciences*, 125:100726, 2021.
- [5] Josue N Rivera and Dengfeng Sun. Air traffic management for collaborative routing of unmanned aerial vehicles via potential fields. In *2024 International Conference on Research in Air Transportation (ICRAT)*, 2024.
- [6] Bizhao Pang, Xinting Hu, Wei Dai, and Kin Huat Low. Uav path optimization with an integrated cost assessment model considering third-party risks in metropolitan environments. *Reliability Engineering & System Safety*, 222:108399, 2022.
- [7] Junghun Suh and Songhwai Oh. A cost-aware path planning algorithm for mobile robots. In *2012 IEEE/RSJ International Conference on Intelligent Robots and Systems*, pages 4724–4729. IEEE, 2012.
- [8] Masaki Nakamiya, Yasue Kishino, Tsutomu Terada, and Shojiro Nishio. A route planning method using cost map for mobile sensor nodes. In *2007 2nd International Symposium on Wireless Pervasive Computing*. IEEE, 2007.
- [9] Aliaksei Pilko, András Söbester, James P Scanlan, and Mario Ferraro. Spatiotemporal ground risk mapping for uncrewed aircraft systems operations. *Journal of Aerospace Information Systems*, 20(3):126–139, 2023.
- [10] Xinting Hu, Bizhao Pang, Fuqing Dai, and Kin Huat Low. Risk assessment model for uav cost-effective path planning in urban environments. *IEEE Access*, 8:150162–150173, 2020.
- [11] Víctor San Juan, Matilde Santos, and José Manuel Andújar. Intelligent uav map generation and discrete path planning for search and rescue operations. *Complexity*, 2018(1):6879419, 2018.
- [12] Luca De Filippis, Giorgio Guglieri, and Fulvia Quagliotti. A minimum risk approach for path planning of uavs. *Journal of Intelligent & Robotic Systems*, 61:203–219, 2011.
- [13] Wei Dai, Bizhao Pang, and Kin Huat Low. Conflict-free four-dimensional path planning for urban air mobility considering airspace occupancy. *Aerospace Science and Technology*, 119:107154, 2021.
- [14] Bizhao Pang, Kin Huat Low, and Chen Lv. Adaptive conflict resolution for multi-uav 4d routes optimization using stochastic fractal search algorithm. *Transportation Research Part C: Emerging Technologies*, 139:103666, 2022.
- [15] Jinjun Rao, Chaoyu Xiang, Jinyao Xi, Jinbo Chen, Jingtao Lei, Wojciech Giernacki, and Mei Liu. Path planning for dual uavs cooperative suspension transport based on artificial potential field-a\* algorithm. *Knowledge-Based Systems*, 277:110797, 2023.
- [16] Ahmed S Abdel-Rahman, Shady Zahran, Basem E Elnaghi, and SF Nafea. Enhanced hybrid path planning algorithm based on apf and a-star. *The International Archives of the Photogrammetry, Remote Sensing and Spatial Information Sciences*, 48:867–873, 2023.
- [17] Lixing Liu, Xu Wang, Xin Yang, Hongjie Liu, Jianping Li, and Pengfei Wang. Path planning techniques for mobile robots: Review and prospect. *Expert Systems with Applications*, 227:120254, 2023.
- [18] Tai Huang, Kuangang Fan, Wen Sun, Weichao Li, and Haoqi Guo. Potential-field-rrt: A path-planning algorithm for uavs based on potential-field-oriented greedy strategy to extend random tree. *Drones*, 7(5):331, 2023.
- [19] Yang Li, Bin Tian, Yuanjun Yang, and Changde Li. Path planning of robot based on artificial potential field method. In *2022 IEEE 6th Information Technology and Mechatronics Engineering Conference (ITOEC)*, volume 6, pages 91–94. IEEE, 2022.



- [20] Seyyed Mohammad Hosseini Rostami, Arun Kumar Sangaiah, Jin Wang, and Xiaozhu Liu. Obstacle avoidance of mobile robots using modified artificial potential field algorithm. *EURASIP Journal on Wireless Communications and Networking*, 2019(1):1–19, 2019.
- [21] Farid Bounini, Denis Gingras, Herve Pollart, and Dominique Gruyer. Modified artificial potential field method for online path planning applications. In *2017 IEEE Intelligent Vehicles Symposium (IV)*, pages 180–185. IEEE, 2017.
- [22] Howie Choset, Ji Y Lee, G.D. Hager, and Z. Dodds. Lecture notes in robotic motion planning: potential functions, 2010.
- [23] Yong K Hwang and Narendra Ahuja. A potential field approach to path planning. *IEEE transactions on robotics and automation*, 8(1):23–32, 1992.
- [24] Xiaojing Fan, Yinjing Guo, Hui Liu, Bowen Wei, and Wenhong Lyu. Improved artificial potential field method applied for auv path planning. *Mathematical Problems in Engineering*, 2020(1):6523158, 2020.
- [25] Cezary Kownacki. Artificial potential field based trajectory tracking for quadcopter uav moving targets. *Sensors*, 24(4):1343, 2024.
- [26] Guoqiang Hao, Qiang Lv, Zhen Huang, Huanlong Zhao, and Wei Chen. Uav path planning based on improved artificial potential field method. *Aerospace*, 10(6):562, 2023.
- [27] Michael Jones, Soufiene Djahel, and Kristopher Welsh. Path-planning for unmanned aerial vehicles with environment complexity considerations: A survey. *ACM Computing Surveys*, 55(11):1–39, 2023.